CHAPTER-IV

THE RELAXATION TIME OF A CHARGE CARRIER DUE TO SCATTERING BETWEEN CHARGE CARRIERS IN A SEMICONDUCTOR SUPERLATTICE

: We have calculated transport relaxation time for an electron ; (i) due to electron-electron scattering in a type-I superlattice and (ii) due to electron-electron and electron-hole scattering in a type-II superlattice, using Fermi-golden rule. The transport relaxation time for a hole due to hole-hole and hole-electron scattering in type-II superlattice is also calculated. Only electron-electron scattering takes place in a type-I superlattice, whereas electron-electron, hole-hole and electron-hole (hole-electron) scattering processes occur in a type-II superlattice. As compared to two-dimensional electron gas, both intralayer and interlayer interactions between charge carriers in a superlattice contribute to transport relaxation time. It is shown that both large momentum transfer scattering as well as small momentum transfer scattering processes contribute to transport relaxation time at all values of temperature and carrier densities. The transport relaxation time of a charge carrier in a superlattice is found larger than that in a three-dimensional free electron gas. The transport relaxation time is found to decrease on increasing temperature, carrier density and single particle energy in sperlattice. We also find that the scattering processes weaken on increasing the width of layer consisting of electrons (holes). The electron-hole (hole-electron) scattering process shows maximum contribution to the transport relaxation time when a hole layer lies exactly in between two consecutive electron layers in a type - II superlattice.

4.1 Introduction

Electron-electron inelastic scattering rate plays an important role in understanding of phenomena such as weak localisation, mesoscopic conductance fluctuation and Aharonov-Bohm effects in nanostructure [1]. Considerable attention has been directed to study the electron-electron relaxation time in low dimensional systems both theoretically and experimentally. Recent progress in haterostructure growth technology also initiated an interest in the electron-electron interaction in pure two-dimensional electron system [2-4] . Theoretically, the effect of the electron-electron interaction on the electron life time was studied by several people [5-11] . While there was a resonable agreement between theoretical prediction and the experimental data for zero temperatures [2] in single quantum well systems, the comparision of the data of the experiments in double-quantum well - systems for finite temperatures [3,4] is more complicated . In strongly - coupled quantum wells (with well separation $d = 14$ Å) the

theory [4] which takes into account the formation of the electron bound states due to quantum tunneling describes the experimental data quite well. In weakly-coupled quantum wells (d= 175-340 Å), for which it is possible [3] to ignore the formation of the electron bound states, theoretical calculations disagree among themselves, and all of them give the inverse electron lifetime less than the experimental data .

The scattering rate obtained from the tunneling experiment [12], with the contribution from the residual impurity scattering excluded, is essentially due to electron-electron interaction. The system of quantum wells (QW'S) coupled by tunneling exhibits a number of interesting properties. For example, the resistance of two QW's with different mobilities connected in paralled strongly depends on the potential profile of the QW's and has a peak when the letter is symmetric [13]. This phenomenon is referred to as resistance resonance (RR) and has been studied to some extent during recent years [14-16] .

Recently, it has been demonstrated (both theoreticaly and experimentally) [17] that in-plane magnetic field suppresses the RR. The magnitude of the effect depends on the coupling energy (Δ) between the wells and also on the width of the single-particle states ($\hbar/\tau$), τ is single particle relaxation time. Experimentally, it has been found that the main temperature dependence of $1/\tau$ is likely to emerge from electron-electron scattering. The comparison of the experimental values of $1/\tau^{ee}$ (as function of temperature) with the well known theoretical expression for the inelastic rate in a two-dimensional electron gas [18] (2 D E G) confirms this assumption. τ^{ee} is contribution to τ from electron-electron scattering. This explanation is quite acceptable when the wells are very weakly coupled and interlayer interactions can be neglected, the electrons are not scattered between the wells. This picture, however, is not valid in the opposite limit of strongly coupled wells. When $\hbar/\Delta$ becomes smaller than any of the time scales in the problem, the staionary states of the electrons are extended over the two wells and the energy spectrum is modified accordingly. Therefore, the theoretical description of $1/\tau^{ee}$ has to be reviewed and compared with the relevant experimental results.

In this chapter, we have calculated relaxation time for an electron from electron-electron scattering in a superlattice of type - I , for an electron due to electron-electron and electron hole scattering and for a hole due to hole-hole and hole-electron scattering in a type-II superlattice, using Fermi-golden rule. Formalism and calculations are given in section 4.2. Our computed results are

discussed in section 4.3 and our work is summarized in section 4.4.

4.2 Formalism and calculations

We use formalism for electron-electron relaxation time, which has been developed by M. Reizer and J. W. Wilkins [19]. This formalism is based on Keldysh diagram technique for inequlibrium processes and it uses the advanced electron Green function .

$$G^A(\rho,\in)=\frac{1}{\in-\xi_p-i\delta}, \tag{4.1}$$

where

$$\xi_p=\frac{\left[p^2-p^2{}_F\right]}{2m}, \tag{4.2}$$

where p_F is the Fermi momentum, m is the electron mass and p is momentum . The electron-electron relaxation time as a function of temperature (T) and single particle energy ($\in$), for a 2 D system is given by [19] .

$$\begin{aligned}\frac{\hbar}{\tau_{e-e}(T,\in)}=\frac{-8}{\pi\nu}\int\frac{dp}{(2\pi)^2}\int\frac{dq}{(2\pi)^3}\left[N(\omega)+n(\omega+\in)\right]\\ \text{x}\ \mathrm{Im}G^A(p,\in)\,\mathrm{Im}G^A\{(p,\in)+(q,\omega)\}\\ \text{x}\ \mathrm{Im}\pi^R(q,\omega)|V(q)|^2,\end{aligned} \tag{4.3}$$

where $\nu=\frac{m}{\pi\hbar^2}$ is the 2D electron density of states. $N(\omega)$ and $n(\in)$ is the Bose and Fermi distribution functions, respectively. The retarded scalar polarization operator is defined as

$$\pi^R(q)=-\nu(1+\frac{i\omega}{qv_F});\qquad \omega\le qv_F\ ,\ q<2_{PF} \tag{4.4}$$

Equation (4.3) can be rewritten as

$$\frac{\hbar}{\tau_{e-e}(T,\in)} = \frac{16}{\pi^2 \nu} \int \frac{d\omega}{2\pi} \omega [N(\omega) + n(\in+\omega)] \int \frac{d^2q}{(2\pi)^2} [V(q)]^2$$

$$\text{x} \left[\int \frac{d^2p}{(2\pi)^2} \text{Im} G^A(p) \, \text{Im} G^A(p+q) \right]^2 . \qquad (4.5)$$

The integral of two Green's functions yields $\left[\frac{\nu\pi}{2\nu_F q}\right]$ and sets the limits for the q integral, $\omega/\nu_F \le q \le 2p_F$. Solutionof Eq.(4.5) yields [19]

$$\frac{\hbar}{\tau_{e-e}(T,\in)} = \frac{2\nu}{\pi^2 \nu_F^{\,2}} \int_0^\infty \omega \, d\omega [N(\omega) + n(\omega + \in)]$$

$$\text{x} \int_{q_0}^{2p_F} \frac{dq}{q} [V(q)]^2 , \qquad (4.6)$$

where V(q) is screened Coulomb potential, $q_o = \omega/\nu_F$ and ν_F is the Fermi velocity. For the case of $\in = 0$ and T is finite, Eq. (4.6) reduces to

$$\frac{\hbar}{\tau_{ee}(T)} = \frac{2\nu}{\pi \nu_F^2} \int_0^\infty \frac{\omega . dw}{\sinh(\hbar\omega/kT)} \int_{q_0}^{2p_F} \frac{dq}{q} [V(q)]^2 \qquad (4.7)$$

Whereas for the case of T = 0 and $\in$ is finite Eq (4.6) goes to

$$\frac{\hbar}{\tau_{e-e}(o,\in)} = \frac{2\nu}{\pi^2 \nu_F^{\,2}} \int_0^\infty \omega . d\omega \int_{q_o}^{2p_F} \frac{dq}{q} [V(q)]^2 \qquad (4.8)$$

In following we evaluate Eq (4.7) and (4.8) for type -I and type-II superlattices.

(A) Type-I Superlattice

The screened Coulomb potential in random phase approximation (RPA) for type-I superlattice, where width of an electron layer (L) is negligibly small as compared the width of unit cell along the direction of growth, d is given by [20]

$$V_1(q) = \frac{2\pi e^2}{q \in_0} \left[\frac{1}{\left\{ 1 + \left(\frac{2}{qa^*}\right)^2 + \left(\frac{4}{qa^*}\right) \coth(qd) \right\}^{1/2}} \right] , \qquad (4.9)$$

where $a^* = \frac{\epsilon_o \hbar^2}{m^* e^2}$ is the effective Bohr radius, and ϵ_0 is background dielectric constant, However, screened Coulomb potential in random phase approximation (RPA) for type-I superlattice, where L is finite and it is comparable with d, is given by

$$V_{1M}(q) = \frac{2\pi e^2}{q\,\epsilon_0}\left[\frac{a}{\sinh(qd)Q}\left\{\frac{\cosh(qd)Q+P}{\sqrt{P^2-Q^2}}-1\right\}+\frac{b}{\sqrt{P^2-Q^2}}\right], \tag{4.10}$$

where

$$P = \mathrm{A_1}\coth(qd)+\mathrm{B_1}, \tag{4.11a}$$

$$Q = -\mathrm{A_1}/\sinh(qd), \tag{4.11b}$$

$$\mathrm{A_1} = 1+\frac{2}{qa_e^*}(H_{ee}-F_{ee}), \tag{4.12}$$

$$\mathrm{B_1} = \frac{2}{qa_e^*}F_{ee}, \tag{4.13}$$

$a = H_{ee} - F_{ee}$ and $b = F_{ee}$ H_{ee} and F_{ee} has been defined earlier by Eqs.(3.11) to (3.15) in chapter- III. .We first evaluate Eq.(4 7) with use of (4.9). It has been argued that in electron-electron scattering major contribution comes from small momentum transfer (small q) [19] In view of that we expanded Eq.(4.9) for $qd<<1$ to obtain

$$V_{1s}(q) \cong \frac{2\pi e^2}{\epsilon_0}\left[\frac{1}{T_1+T_2q^2-T_3q^4}\right]^{1/2}, \tag{4.14}$$

where

$$T_1 = 4\left[\frac{1}{a^*}+\frac{1}{a^*d}\right], \tag{4.15}$$

$$T_2 = 1+\frac{4d}{3a^*}, \tag{4.16}$$

$$T_3 = \frac{4d^3}{45}. \tag{4.17}$$

As is obvious from Eq. (4.7), ω-integration mainly contribute for smaller ω-values in the range $0 \le \omega \le {}^{k_B T}/_{\hbar}$. We replace $V(q)$ by $V_{1s}(q)$ in Eq.(4.7) and then perform integration over q for $q_0 \le q \le 2P_F$ and over ω for $0 \le \omega \le \frac{k_B T}{\hbar}$ to get

$$\frac{\hbar}{\tau_{1s}(T,0)} = \frac{Tk_F d^2}{2\in_F}\left[\frac{Tk_F}{2\in_F}\left\{a_1 \ln\left(\frac{4p_F{}^2 - y_1}{4p_F{}^2}\right) - a_2 \ln\left(\frac{4p_F{}^2 - y_2}{4p_F{}^2}\right)\right\}\right.$$
$$+(a_1 - a_2)x\left\{\frac{Tk_F}{2\in_F}\ln\left(\frac{Tk_F}{2\in_F}\right)^2 - \frac{Tk_F}{\in_F}\right\}$$
$$-a_1\left\{\frac{Tk_F}{2\in_F}\ln\{(Tk_F/\in_F)^2 - y_1\}\right\} - \frac{Tk_F}{\in_F} - \sqrt{y_1}$$
$$x\ \ln\left\{\frac{(Tk_F/2\in_F) - \sqrt{y_1}}{(Tk_F/2\in_F) + \sqrt{y_1}}\right\} + a_2\left\{\frac{Tk_F}{2\in_F}\ln\left\{(Tk_F/2\in_F)^2 - y_2\right\}\right\}$$
$$\left.-\frac{Tk_F}{\in_F} - \sqrt{y_2}\quad x\ln\left\{\frac{(Tk_F/2\in_F) - \sqrt{y_2}}{(Tk_F/2\in_F) + \sqrt{y_2}}\right\}\right], \tag{4.18}$$

where

$$\in_F = {}^{\hbar^2 k_F{}^2}/_{2m} \text{ and } k_F = \sqrt{2\pi n_s}$$

$$a_1 = \frac{16}{(a^* k_F)^2 \pi}\frac{1}{T_3\sqrt{(T_2/T_3)^2 + 4(T_1/T_3)}}\frac{1}{y_1}\ , \tag{4.19}$$

$$a_2 = \frac{16}{(a^* k_F)^2 \pi}\frac{1}{T_3\sqrt{(T_2/T_3)^2 + 4(T_1/T_3)}}\frac{1}{y_2}\ , \tag{4.20}$$

$$y_1 = \left[\frac{(T_2/T_3) + \sqrt{(T_2/T_3)^2 + 4(T_1/T_3)}}{2}\right] \tag{4.21}$$

$$y_2 = \left[\frac{(T_2/T_3) - \sqrt{(T_2/T_3)^2 + 4(T_1/T_3)}}{2}\right]. \tag{4.22}$$

The results on $\frac{\hbar}{\tau_{1s}(T)}$ from Eq.(4.18) and from numerical integration over ω and q in Eq.(4.7) and (4.8) with the use of Eqs.(4.9) and (4.10) will be discussed in section 4.3.

(B) Type-II Superlattice

Screened coulomb potential in random phase approximation (RPA) for type-II superlattice, where width of an electron layer (L_e) and of a hole layer (L_h) is much smaller as compared to d, is given by [20] .

$$V_2(q)=\frac{4\pi e^2}{q\in_0}\left[\frac{1+2F(q)/q\left[\frac{1}{a_1^*}+\frac{1}{a_2^*}\right]+g(q)}{\left[1+R^2(q)+2R(q)\coth(qd)\right]^{1/2}}-\sinh(qd_1)\right], \tag{4.23}$$

where

$$F(q)=\frac{\cosh(qd)-\cosh(qd')}{\sinh(qd)} \tag{4.24}$$

$$g(q)=\cosh(qd_1)+\sinh(qd_1)R(q), \tag{4.25}$$

and

$$R(q)=\frac{2}{q}\left[\frac{1}{a_1^*}+\frac{1}{a_2^*}\right]+\frac{4F(q)}{q^2a_1^*a_2^*} \tag{4.26}$$

The screened Coulomb potential in RPA for type-II compositional superlattice, where L_e and L_h are comparable with d, is given by

$$V_2'(q)=\left(\frac{2\pi e^2}{q\in_0}\right)^2\left[\frac{R}{\in}+\frac{C}{\in}\right] \tag{4.27}$$

Where

$$\frac{R}{\in}=\left[\frac{\beta_0}{\sqrt{\cosh(qd)^2-1}}+\frac{\beta_1}{\sqrt{\left(r_0+\cosh(qd)\right)^2-1}}\right] \tag{4.28}$$

with

$$\beta_0 = \frac{B_1\ (\sinh(qd))^2}{pr_0}, \tag{4.29}$$

$$B_1 = \frac{2}{qa_e^*}\left(F_{110} - F_{120}\right) + \frac{2}{qa_h^*}\left[F_{220} - F_{210}\right], \tag{4.30}$$

$$r_0 = \frac{q\sinh(qd)}{P}. \tag{4.31}$$

The P and Q are defined as

$$P = 1 + \frac{2}{qa_e^*}(H_{ee} - F_{ee}) + \frac{2}{qa_h^*}(H_{hh} - F_{hh}) + \frac{4}{q^2 a_e^* a_h^*}$$

$$(H_{ee}\ H_{hh} - F_{ee}\ H_{hh} - H_{ee}\ F_{hh} + F_{ee}\ F_{hh}); \tag{4.32}$$

$$Q = \frac{2}{qa_e*}F_{ee} + \frac{2}{qa_h*}F_{hh} + \frac{4}{q^2\ a_e*a_h*}\{(F_{ee}H_{hh} + H_{ee}F_{hh})$$

$$-2F_{ee}\ F_{hh}\ +\ F_{eh}\ F_{he}\ F\}\ , \tag{4.33}$$

$$F = \frac{\cosh(qd) - 1}{\sinh(qd)} \tag{4.34}$$

H_{ee}, H_{hh}, F_{ee}, F_{hh} & F_{eh}, F_{he} are defined in chapter - III by equations (3.13) to (3.15).

The β_1 is defined as

$$\beta_1 = \frac{A_1 \sinh(qd)}{P} - \frac{\beta_1(\sinh(qd))^2}{\mathrm{Pr}_0} \tag{4.35}$$

with

$$A_1 = 2 + \frac{2}{qa_e^*}(H_{ee} - F_{ee}) + \frac{2}{qa_h^*}(H_{hh} - F_{hh}) \quad + F\left(\frac{2}{qa_e^*}\ F_{120} + \frac{2}{qa_h^*} F_{210}\right) . \qquad (4.36)$$

Further,

$$\frac{C}{\in} = \left[2 + 2/qa_e^*(H_{ee} - F_{ee}) + 2/qa_h^*(H_{hh} - F_{hh})\right]$$

$$\text{x}\left[\sinh(qd_1)\ I_0 + \sinh(q(d-d_1))x\ I_1\right] + \left\{\frac{2}{qa_e^*}(F_{ee} - F_{eh}) + \frac{2}{qa_h^*}(F_{hh} - F_{he})\right\}$$

$$\text{x}[\sinh(\text{qd}_1)\sinh(\text{qd})\ \text{I}_2 + \sinh \text{q(d-d}_1)\text{x}\sinh(\text{qd})\ \text{I}_1] \quad , \qquad (4.37)$$

where

$$I_0 = \frac{1}{P}\left[\frac{(\cosh(qd) + r_0)}{\sqrt{(\cosh(qd) + r_0)^2 - 1}} - 1\right] , \qquad (4.38)$$

$$I_1 = \frac{1}{P\sqrt{(\cosh(qd) + r_0)^2 - 1}} , \qquad (4.39)$$

$$I_2 = \frac{1}{\text{Pr}_0}\left[\frac{\cosh(qd)}{\sqrt{(\cosh(qd))^2 - 1}} - \frac{(\cosh(qd) + r_0}{\sqrt{(\cosh(qd) + r_0)^2 - 1}}\right] . \qquad (4.40)$$

4.3 Results and Discussion

For discussion of results on τ_{ee} (T, $\in$) we divide the section in two parts. The computed τ_{ee} for type-I superlattice (τ_1) as the function of T and $\in$ is discussed first past, whereas τ_{ee} for type-II superlattice (τ_2) is discussed in second part.

(A) Results on τ_1

We computed τ_1 as a function of T :(i) using Eq.(4.18), (ii) performing numerical integration over ω and q in Eq.(4.7) by making use of Eq.(4.9) and (iii) performing numerical integration over ω and q in Eq.(4.7) by making use of Eq.(4 10). In following, above mentioned three values of τ_1 are

called $\tau_{1s}(T)$, $\tau_{1nm}(T)$, and $\tau_{1m}(T)$ respectively. Computed $\hbar/\tau_{1s}\in_F$, $\hbar/\tau_{1NM}\in_F$ and $\hbar/\tau_{1M}\in_F$ are plotted as function of x(=$k_B T/\in$) in Fig.4.1, for GaAs/A1$_x$ Ga$_{1-x}$ As superlattice which has been modelled in terms of following values of parameters : $n_s = 7.3 \times 10^{11}$ cm^{-2}, $m_e^* = 0.068\ m_e$, d=500 Å, L = 200 Å and $\in_0 = 13.1$. n_s is the number of carrier per unit area. The results from experimental data [3] and from earlier calculations of τ_{e-e} for a two-dimensional gas [19] are also plotted in Fig. 4.1 for comparision with our results. As can be seen from the figure; (i) $\hbar/\tau_{1s}$ is larger than $\hbar/\tau_{1NM}$ and $\hbar/\tau_{1M}$ for all values of T and (ii) $\hbar/\tau_{1NM} > \hbar/\tau_{1M}$ for all values of T. τ_{1s} and τ_{1NM} both are computed for the case of width of an electron layer is negligibly small as compared to the length of the unit cell. However τ_{1s}, unlike τ_{1NM}, incorporates the contributions only from electron-electron scattering processes which take place for smaller q ($qd \langle\langle 1$). Comparision of τ_{1s} and τ_{1NM} suggest that it is not quite correct to say that electron-electron scattering mainly contribute for small momentum transfer processes. The ratio τ_{1s}/τ_{1NM} has been plotted as a function of x in Fig 4.2. Figure 4.2 suggests that large momentum transfer electron-electron scattering processes contribute more at small temperature ($T \leq 30K$). For T > 30K contribution from large momentum transfer electron-electron scattering processes is nearly 25 % that of small momentum transfer electron-electron scattering processes.

Comparision of our computed $\hbar/\tau_{1NM}$ with $\hbar/\tau_{e-e}$ for two dimensional electron sheet suggest that interlayer interaction, which is present in type-I superlattice and is absent in a 2D electron sheet, contributes significantly at all temperatures. However this contribution depends on length of the unit cell d. As can be seen from Fig.4.3, contribution from interlayer interaction to electron-electron scattering increases on decreasing d. For $d \to 0$ (small d-values) the superlattice structure approaches to a 3D free electron gas system, whereas for $d \to \infty$ (large d- value) the superlattice structure tends to 2D free electron gas. As it should be, our computed $\hbar/\tau_{1s}$ almost merges with $\hbar/\tau_{e-e}$ for 2D free electron gas for d= 2000 Å. An interesting point which merges out of Fig. 4.3 is the stronger electron-electron interaction in 2D free electron gas as compared to that in 3D free electron gas. Comparision between $\hbar/\tau_{1NM}$ and $\hbar/\tau_{1M}$ in Fig. 4.1 suggests that increase in width of an electron layer enhances the relaxation time for electron-electron scattering. The electron-electron scattering weakens on increasing width of the layer consisting of electron, as expected.

Figure 4.4 shows plot of $\hbar/\tau_{1NM}\in_F$ as a function of x for three values of n_s (=3 x 10^{11} cm^{-2}, 5 x 10^{11} cm^{-2}, 7.3 x 10^{11} cm^{-2}). It can be inferred from the figure that electron-electron scattering relaxation time decreases with increasing number of electron per unit area in a superlattice. Looking at figure 4.1

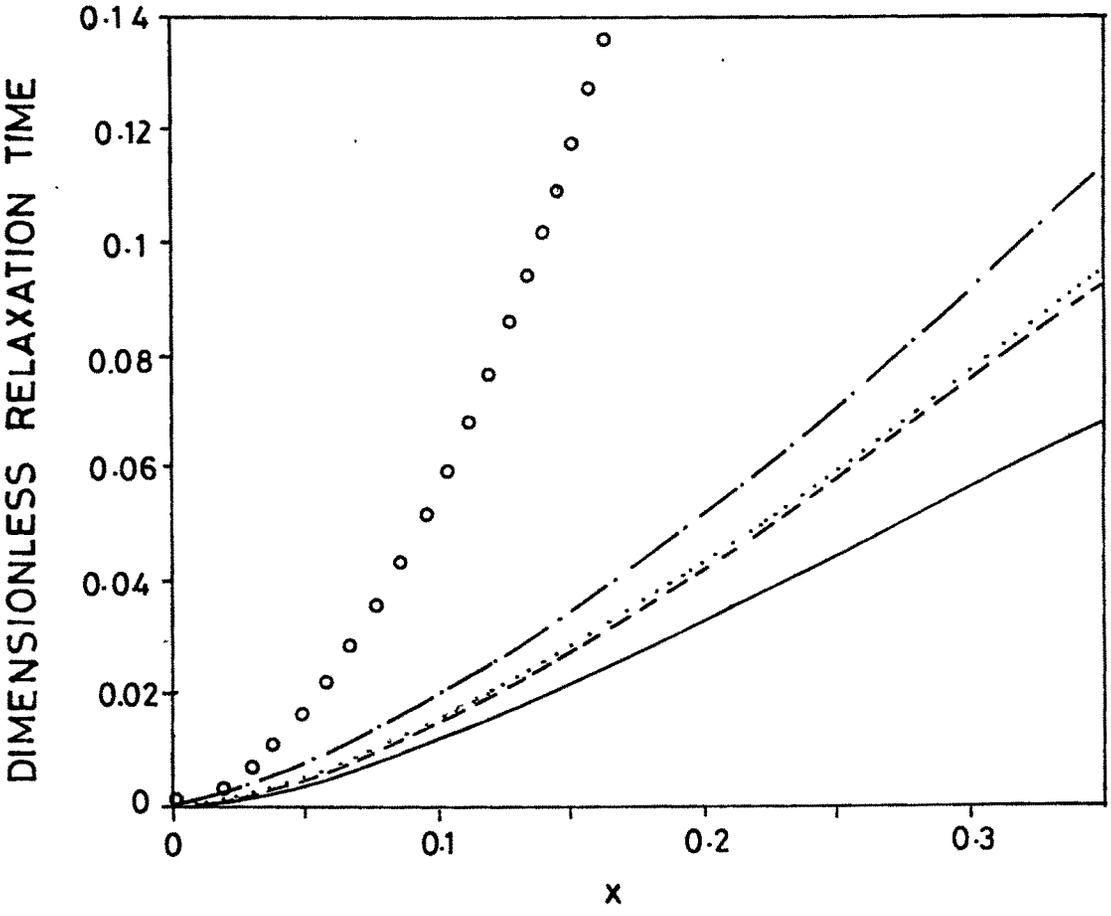

Fig.4.1 Plot of dimensionless electron relaxation time as a function of $x=k_BT/\varepsilon_F$. Experimental result (open circles), our results $\hbar/\tau_{1s}\varepsilon_F$ (dash-dot line), $\hbar/\tau_{1NM}\varepsilon_F$ (dash-dash line), $\hbar/\tau_{1M}\varepsilon_F$ (solid line) and results from Ref. [19] (dot-dot line).

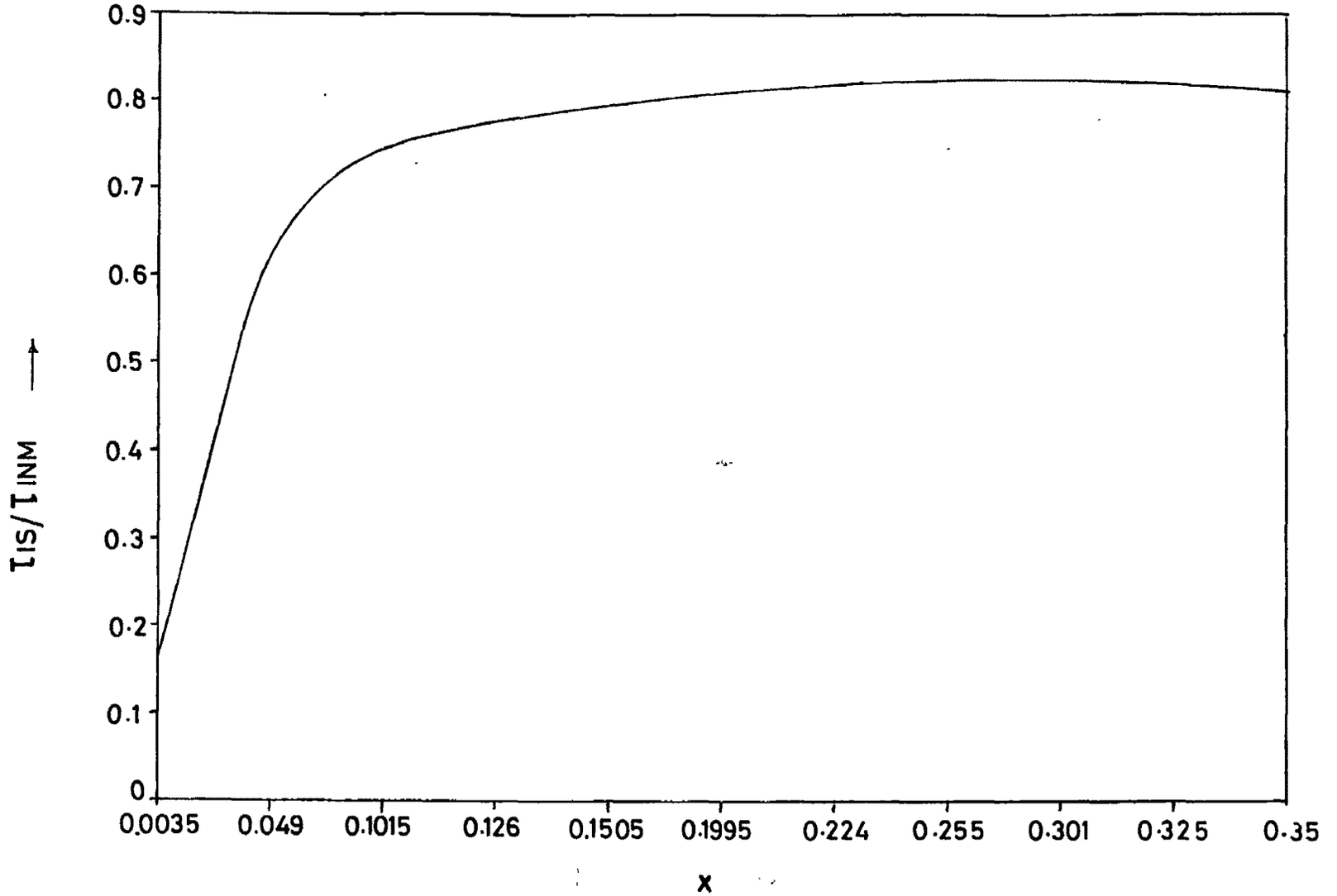

Fig.4.2 Plot the ratio (τ_{1s}/τ_{1NM}) as a function of $x=k_BT/\varepsilon_F$.

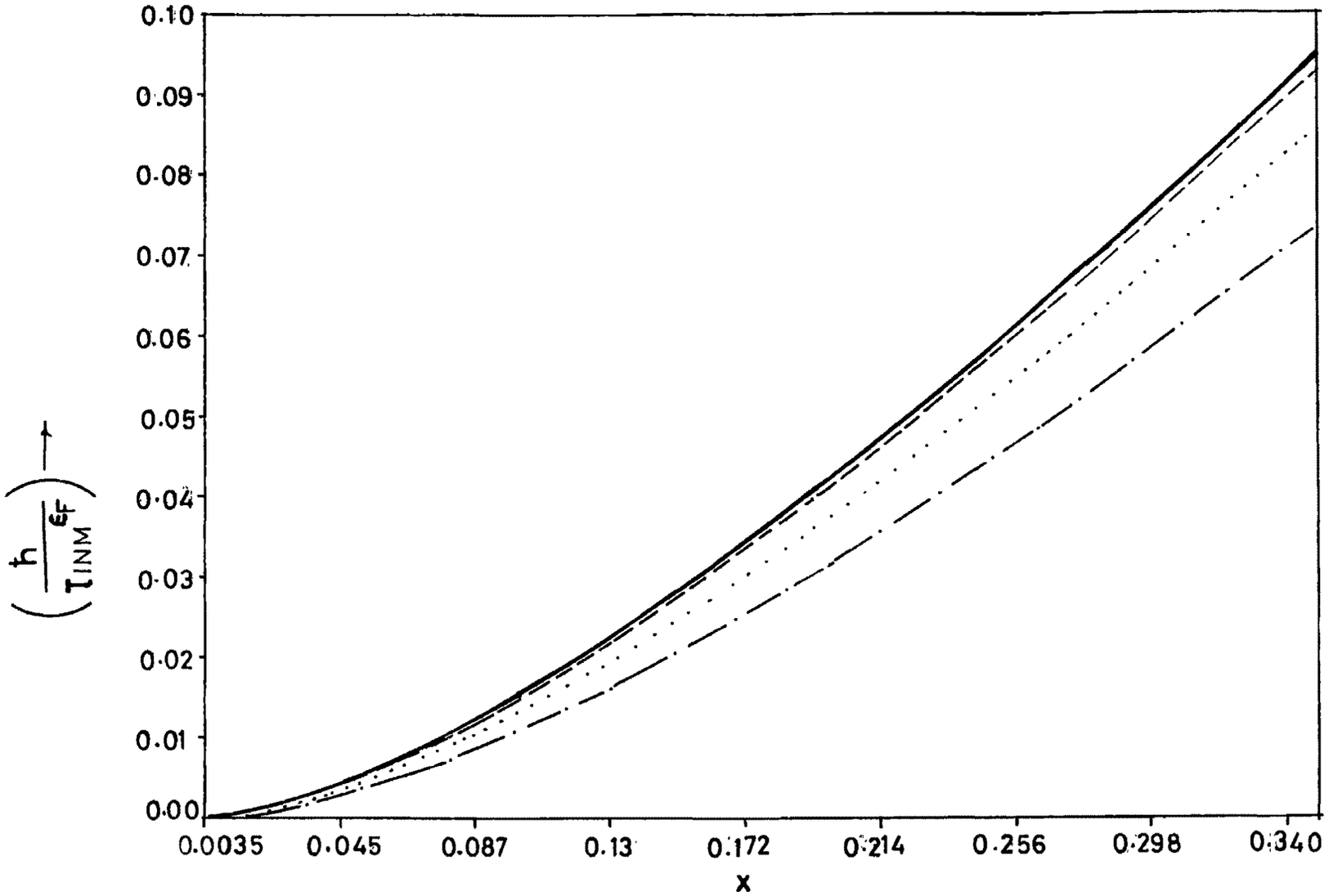

Fig.4.3 Plot of $\hbar/\tau_{1NM}\epsilon_F$ as a function of x, for d=100Å (dash-dash line), d=200Å (dot-dot line), d=500Å (dash-dash line) and d=1000Å as well as d=2000Å (solid line).

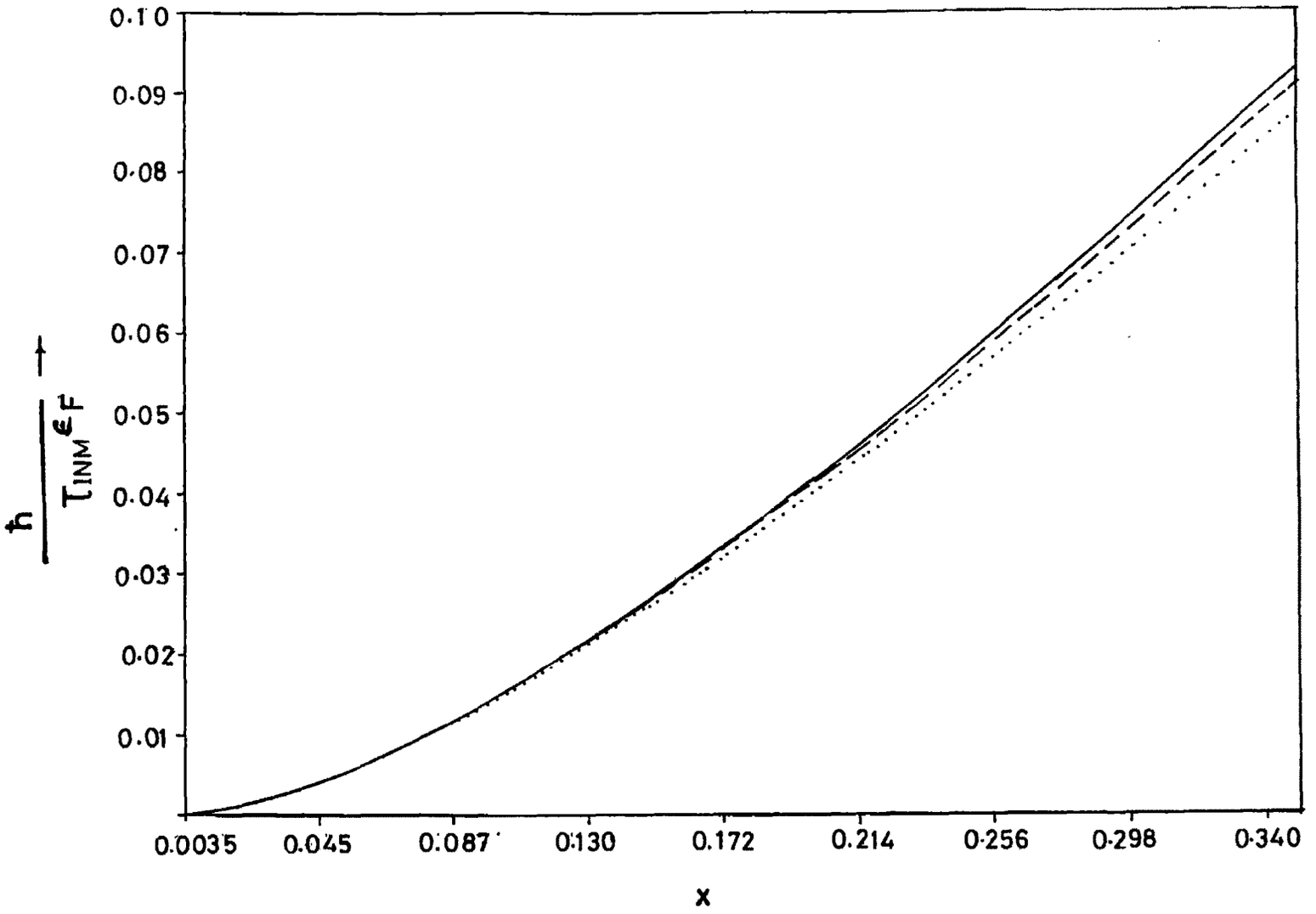

Fig.4.4 Plot of $\hbar/\tau_{1NM}\epsilon_F$ as a function of x, for $n_{se}=3x10^{11}cm^{-2}$ (dot-dot line), $n_{se}=5x10^{11}cm^{-2}$ (dash-dash line) and the $n_{se}=7x10^{11}cm^{-2}$ (solid line).

to 4.4 we notice that electron-electron relaxation time can be much larger to make significantly contribution to mobility at lower temperature (T<10K). A rough estimate of mobility due to electron-electron scattering can be made using $\mu_e = \frac{e\tau_{ee}}{m}$, which can be reasionably high for T <10K. It can therefore be concluded that electron-electron scattering plays an important role in determining the transport properties of low dimesional systems such as semiconductor superlattices at small T-values, where electron-phonon scattering become insignificant.

Our computed $\hbar/\tau_1(\in) \in_F$ from Eq.(4.8) by making use of Eq.(4.9) is plotted as a function of $\in$ in Fig. 4.5 .The resutls from calculation of Reizer and Wilkins are also plotted for comparision with our results. As is seen from the figure, variation of $\hbar/\tau_1 \in_F$ with $\in$ is very similar to that of $\hbar/\tau_{1NM} \in_F$ versus T. The figure suggests that electron-electron scattering becomes faster on increasing $\in$. Also, the comparision of our calculations with that of Reizer and Wilkins shows that interlayer interactions contribute significantly for all values of $\in$. This contribution is larger at smaller values of $\in$. It is to be mentioned that in obtaining the results plotted in Figs. (4.1) to (4.5) a numerical computation of $\hbar/\tau_{1NM} \in_F$, $\hbar/\tau_1 \in_F$ and $\hbar/\tau_1(\in) \in_F$ has been made by performing double intergration in Eq. (4.7) and Eq.(4.8) using Gaussian qudrature method.

(B) Results on τ_2

The transport relaxation time for electrons and for holes in InAs/GaSb type -II superlattice have been calculated by making use of Eqs.(4.23) to (4.26) in Eq. (4.7) and then by performing double integration over q and ω. The InAs/GaSb superlattice has been modelled in terms of following values of parameters: ε_0 (InAs) = 12.3, ε_0 (GaSb) = 14.4, $m_e^* = 0.026me$, $m^*_h = 0.3$me, d=1000Å. Type-II Superlattice consists of electron-electron scattering, hole-hole scattering and electron-hole scattering, whereas type-I superlattice consists of electron-electron scattering only. The relaxation time of an electron is therefore contributed by electron-electron scattering and electron-hole scattering. Similarly the relaxation time for a hole is contributed by hole-hole scattering and by hole-electron scattering in a type-II superlattice. The contribution from electron-hole scattering or hole-electron scattering is governed by the separation (d_1) between an electron layer and a hole layer in a unit cell. In order to see how the change in d_1 affects the relaxation time of an electron (τ_{2e}) and relaxation time of a hole (τ_{2h}), we have computed $\hbar/\tau_{2e} \in_F$ and $\hbar/\tau_{2h} \in_F$ as a function of T at $n_{se} = n_{sh} = 5 \times 10^{11}$ cm^{-2} for four values of d_1 (=100 Å, 300 Å, 500 Å and 700 Å), for InAs/GaSb superlattice using

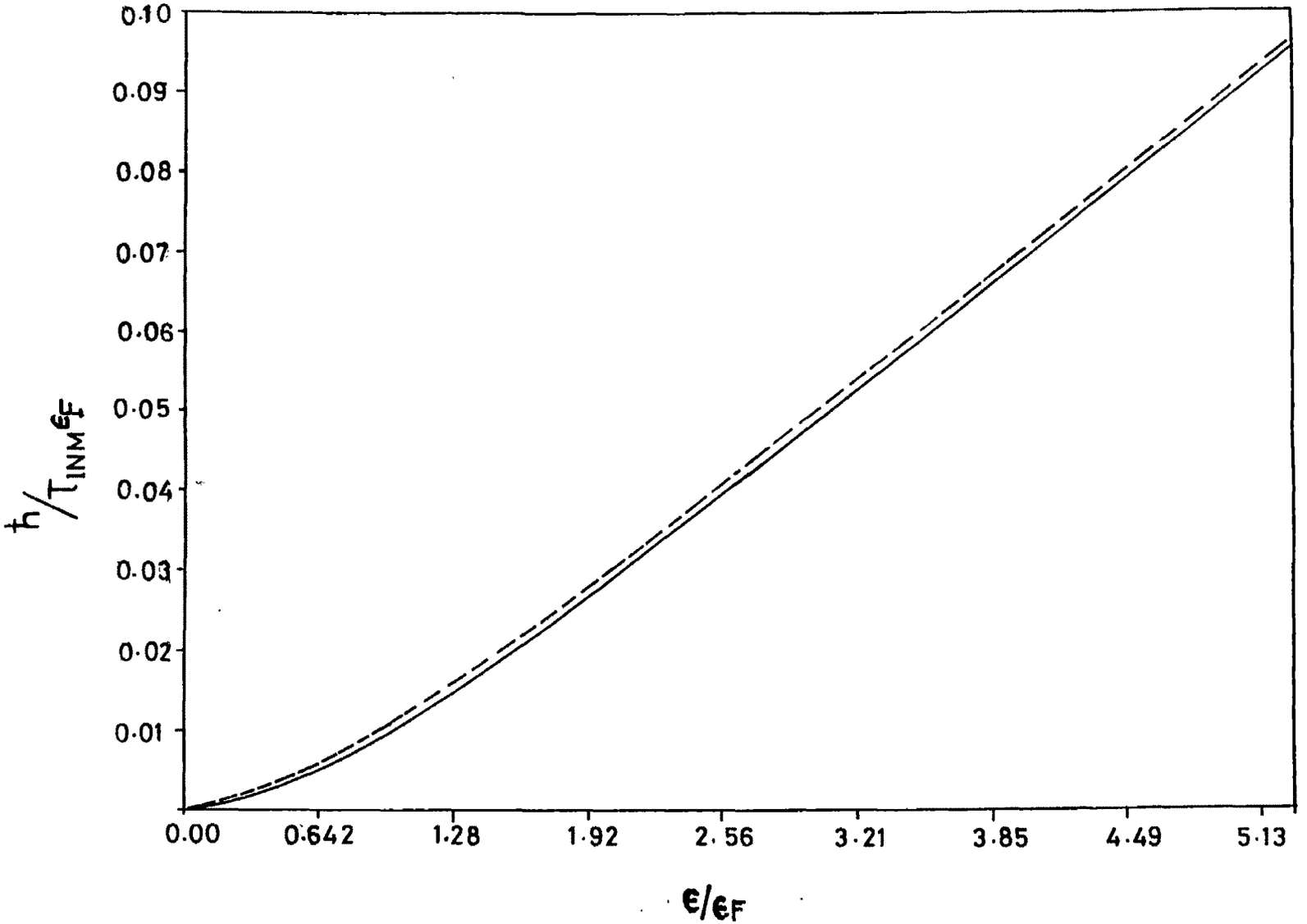

Fig.4.5 Plot of $\hbar/\tau_{1NM}\varepsilon_F$ as a function of energy $\varepsilon/\varepsilon_F$. Results from Ref.[19] (dash-dash line) and our results (solid line).

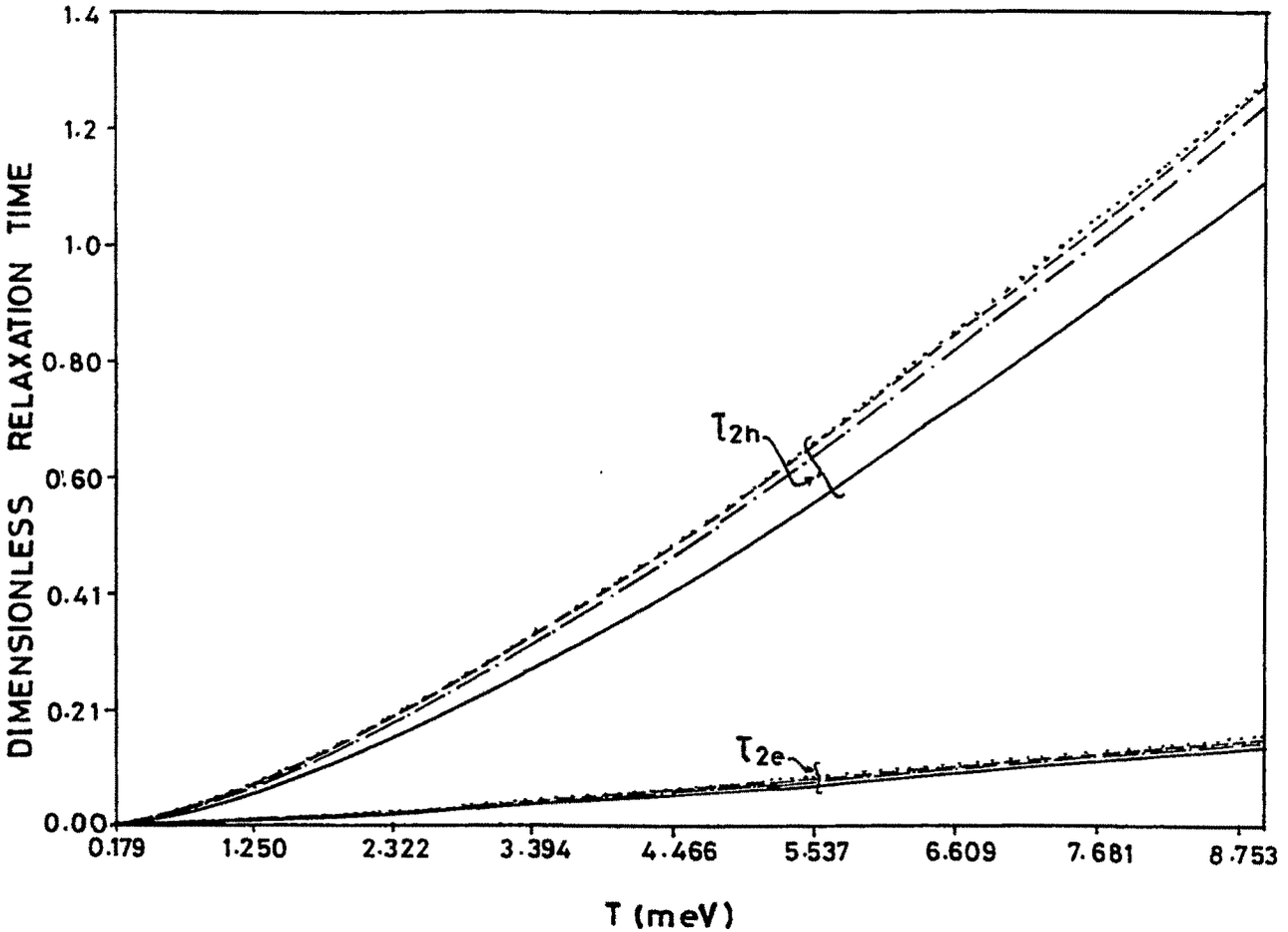

Fig.4.6 Plot of dimensionless electron and hole relaxation time as a function of temperature. $\hbar/\tau_{2h}\varepsilon_F$ as a function of T (upper curves) for d_1=100Å (solid line), d_1=300Å (dash-dash line), d_1= 500Å (dot-dot line) and d_1= 700Å (dot-dash line). $\hbar/\tau_{2e}\varepsilon_F$ as a function of T (lower curves), for d_1=100Å (solid line), d_1=300Å (dash-dash line), d_1= 500Å (dot-dot line) and d_1= 700Å (dot-dash line).

Eqs.(4 23) to (4.26) in Eq. (4.7). The n_{se} and n_{sh} are the number of electrons and number of holes per unit area, respectively. We have taken $\in_F = (\in_{Fe} + \in_{Fh})/2$, where $\in_{F_e}$ ($\in_{Fh}$) is the Fermi energy of electrons (holes). Our computed $\hbar/\tau_{2e} \in_F$ and $\hbar/\tau_{2h} \in_F$ decrease on increasing d_1 when $d_1 \leq d/2$, for all values of d. However, they start declining on increasing d_1 for $d_1 > d/2$. The maximum value $\hbar/\tau_{2e} \in_F$ and $\hbar/\tau_{2h} \in_F$ is obtained when $d_1 = d/2$ at all temperature. In type-II superlattice a hole layer lies in between two electron layers. The Fig.4.6 suggests that τ_{2e} has minimum value when the hole layer lies exactly in between two electron layers and it start increasing as soon as the electron layers shifts towards any one of the two electron layers. We thus find that electron -hole scattering makes a minimum contribution when a hole layer lies exactly in between two adjoing electron layers. Same conclusion apply to the hole-electron scattering which contributes to τ_{2h}.

In order to see how the change in n_{se} and n_{sh} at a fixed value of d_1 affects the τ_{2e} and τ_{2h}, we have computed τ_{2e} and τ_{2h} as a function T at $d_1 = 400$ Å for three values of n_{se} (=3 x 10^{11} cm^{-2}, 5 x 10^{11} $c\,m^{-2}$ & 7 x 10^{11} cm^{-2}) and three values of n_{sh} (=3 x 10^{11} cm^{-2}, 5 x 10^{11} cm^{-2}, & 7 x 10^{11} cm^{-2}) using Eqs. (4.23) to (4.26) in Eq. (4.7). Our computed results are plotted in Fig.4.7. The figure suggests that both $\hbar/\tau_{2e} \in_F$ increases on increasing n_{se} at all temperature T-values. Similarly $\hbar/\tau_{2h} \in_F$ increases on increasing n_{sh} at all T-values. This can be attributed to the simple fact that probability of electron-electron scattering and that of electron-hole scattering increases on increasing n_{se}, whereas probability of hole-hole and hole-electron scattering increases on increasing n_{sh}.

We have also computed τ_{2e} and τ_{2h} by making use of Eqs (4.27) to (4.40) in Eq.(4.7), in order to see the effect of increase in width of a layer consisting of electrons (holes). It is found that the effect of change in width of a layer on electron-electron, hole-hole and electron-hole scattering in a type-II superlattice is similar to the effect of change in a width of layer on electron-electron scattering in type-I superlattice.

4.4 Summary

We have calculated $\tau_{1s}(T)$, $\tau_{1NM}(T)$, $\tau_{1M}(T)$ for GaAs/Al_xGa_{1-x} As superlattice. We find that $\hbar/\tau_{1s} > \hbar/\tau_{1NM}$ and $\hbar/\tau_{1NM} > \hbar/\tau_{1M}$ for all values of d_1. By comparing our computed τ_{1s} and τ_{1NM}, we conclude that large momentum transfer electron-electron processes make significantly large contribution to the relaxation time at small T-values ($T \leq 30K$). For T > 30K contribution from large

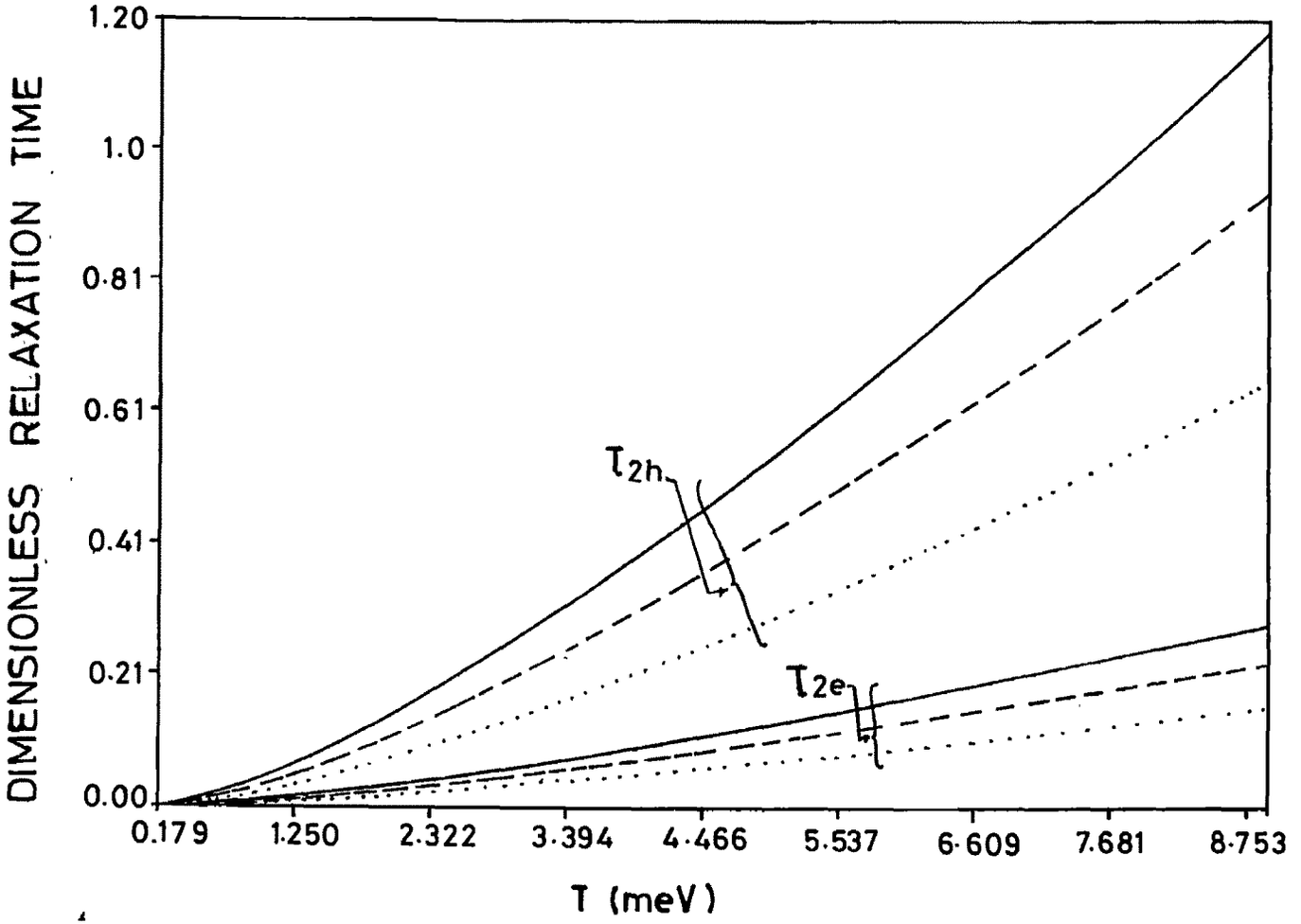

Fig.4.7 Plot of dimensionaless relaxation time as a function of $T.\hbar/\tau_{2h}\varepsilon_F$ as a function of T (upper curves) for $n_{se}=3x10^{11}cm^{-2}$ (dot-dot line), $n_{se}=5x10^{11}cm^{-2}$ (dash-dash line) and the $n_{se}=7x10^{11}cm^{-2}$ (solid line). $\hbar/\tau_{2e}\varepsilon_F$ as a function of T (lower curves) for $n_{sh}=3x10^{11}cm^{-2}$ (dot-dot line), $n_{sh}=5x10^{11}cm^{-2}$ (dash-dash line) and the $n_{sh}=7x10^{11}cm^{-2}$ (solid line).

momentum electron-electron scattering processes is nearly 25 % that of small momentum transfer electron-electron scattering processes. τ_{1NM} reduces to value of τ_{e-e} for 2 DFEG for $d \to \infty$ (very large value of the d), whereas it reduces to value of τ_{e-e} for 3DFEG for $d \to 0$ (small value of d). τ_{1NM} is smaller than the τ_{e-e} for 3DFEG for all values of T, which suggests that electron-electron scattering plays an important role in determining the transport relaxation time for an electron when effective dimension of a system reduces. Comparision between our computed τ_{1NM} and τ_{1M} suggests that increase in width of an electron layer enhances the relaxation time for electron-electron scattering. We also find that electron-electron scattering relaxation time decreasing on increasing number of electrons per unit area in a superlattice . The behaviour of our computed τ_{1NM} as a function of $\in$ is found very similar to its behaviour with T.

We computed τ_{2e} and τ_{2h} for InAs/GaSb superlattice . We find that $\hbar/\tau_{2e}$ has maximum value when the hole layer lies exactly in between two electron layers and it start increasing as soon as the electron layers shifts towards any one of the two electron layers. Same conclusion apply to the hole-electron scattering which contributes to τ_{2h} . We further find that $\hbar/\tau_{2e}$ increases on increasing n_{se} at all temperature T-values. On increasing the width of a layer consisting of electrons (holes) τ_{2e} (τ_{2h}) increases at all values of T and n_{se} (n_{sh}).

References

[1] B. L. Altushuler nad A.G.Arnov, in *Electron-Electron Interaction in Disordered Systems,* edited by A. L. Efros and M. Polak (North -Holland, Amsterdam, 1985).

[2] A. Yacoby, U. Sivan, C.P. Umbach, and J. M. Hong, Phys. Rev. Lett. **66**, 1938 (1991) ; A. Yaco by , M. Heiblum, H. Strikman, V. Umansky, and D. Mahalu, semicond. Sci. Technol. **9**, 907 (1994).

[3] S. Q. Murphy, J P. Eisentein, L.N. Pfeffer, and K.W. West, Phys. Rev. **B 52**, 14825 (1996).

[4] M. Slutzky, O. Entin-Wohlman, Y. Berk, A. Polevsky, and H. Shtrikannan, Phys. Rev. **B 53**, 4055 (1996).

[5] C. Hodges, H.Smith and J.W. Wilkins, phys. Rev. **B4**, 302 (1971).

[6] A.V. Chaplik, Zh. Eksp. Teor. Fiz. **60**, 1845 (1971) [Sov. Phys. JETP **33**, 997 (1971)].

[7] G.F. Giuliani and J.Quinn, Phys. Rev. **B 26** , 4421 (1982).

[8] H. Fukuyama and E. Abrahams, Phys. Rev. **B 27**, 5976 (1983).

[9] J. Rammer and H. Smith, Rev. Mod. Phys. **58**, 323 (1986).

[10] L. Zhong and S.Das Sarma, Phys. Rev. **B 53**, 9961 (1996).

[11] T. Jungwirth and A. H. MacDonald, Phys. Rev. **B 53**, 7403 (1996).

[12] S. Q. Murphy, J. P. Eisentein, L. N. Pfeciffer, and K.W. West, Phys. Rev. **B 52**, 14825 (1995).

[13] A. Palevski, F. Beltram, F. Capasso, L. N. Pfeiffer, and K.W. West, Phys. Rev. Lett. **65**, 1929 (1990).

[14] A. Palevski, S. Luryi, P. L. Gammel, F. Capasso, L. N. Pfeiffer and K.W. West, Superlattice Microstruct, **11**. 269 (1992).

[15] Y. Ohno, M. Tsuchia, and H. Sakaki, Appl. Phys. Lett. **62**, 1952 (1993).

[16] Y. Berk, A. Kamenev, A. Palevski, L. N. Pfeiffer, and K.W. West, Phys. Rev. **B 50**, 154 (1994).

[17] Y. Berk, A. Kamenev, A. Palevski, L. N. Pfeiffer, and K.W. West, Phys. Rev. **B 51**, 2604 (1995).

[18] G. F. Giuliani and J. J. Quinn, Phys. Rev. **B 26**, 4421 (1982).

[19] Michael Reizer and John W. Wilkins, Phys. Rev. **B 55,** R7363 (1996).

[20] A. C. Sharma, Solid State Commn. **95**, 569, (1995).